

Particle distributions and X-ray spectra in single or multiple solar current sheets

C. Gontikakis,¹★ A. Anastasiadis²★ and C. Efthymiopoulos¹★

¹Research Centre for Astronomy and Applied Mathematics, Academy of Athens, Soranou Efessiou 4, 115 27 Athens, Greece

²National Observatory of Athens, Institute for Space Applications & Remote Sensing, 15236 Palaia Penteli, Greece

Accepted 2007 April 5. Received 2007 April 3; in original form 2007 February 22

ABSTRACT

The acceleration of charged particles in a site of magnetic reconnection is analysed by detailed numerical simulations. Single or multiple encounters of the particles with Harris-type reconnecting current sheets (RCSs) are modelled as an overall stochastic process taking place within an active region. RCS physical parameters are selected in a parameter space relevant to solar flares. Initially, the charged particles form a thermal (Maxwellian) distribution corresponding to coronal temperature $\simeq 2 \times 10^6$ K. Our main goal is to investigate how the acceleration process changes the shape of the particles' kinetic energy distribution. The evolution of the kinetic energy distribution, calculated numerically after one encounter of the particles with a single RCS, is found to be in good agreement with our previously published analytical formulae. In the case of consecutive encounters, we find that the kinetic distribution tends to converge to a practically invariant form after a relatively small number of encounters. We construct a discrete stochastic process that reproduces the numerical distributions and we provide a theoretical interpretation of the asymptotic convergence of the energy distribution. We finally compute the theoretical X-ray spectra that would be emitted by the simulated particles in a thick target model of radiation.

Key words: acceleration of particles – radiation mechanisms: non-thermal – Sun: flares – Sun: X-rays, gamma-rays.

1 INTRODUCTION

The study of the particle acceleration process during solar flares still remains an important and open issue. The acceleration of ions and electrons is the result of the energy release process occurring in these highly energetic events, in which the magnetic energy is converted, through magnetic reconnection, into heating, bulk motion of the flaring plasma and particle acceleration.

In the framework of the above scenario, and on the basis of the early work of Speiser (1965) for the proton acceleration during reconnection in the Earth's magnetotail, Martens (1988) and Martens & Young (1990) argued that the flaring coronal medium is also effectively collisionless so that the Speiser mechanism could be applied to the particle acceleration during flares. In particular, similarly to the Earth magnetotail, in solar flares it is possible that the particles be accelerated by super-Dreicer electric fields. Litvinenko & Somov (1993) and Litvinenko (1996) studied the particle acceleration in non-neutral reconnecting current sheets (RCSs) proposing scaling formulae for the kinetic energy gain of the particles. In two recent papers Efthymiopoulos, Gontikakis & Anastasiadis (2005)

and Gontikakis, Efthymiopoulos & Anastasiadis (2006), we studied in detail the dynamics of particles orbiting in an RCS, and found general formulae for the kinetic energy gain of the particles that contain Speiser's and Litvinenko's formulae as asymptotic limits.

Further insight to this problem can be obtained by taking an initially thermal distribution of particles at coronal temperature and by simulating numerically the acceleration process. Zharkova & Gordovskyy (2004) and Wood & Neukirch (2005) studied simulations of particles with a thermal initial distribution, that are subsequently accelerated by non-neutral Harris-type RCSs. These authors concluded that the accelerated particles form, in general, narrow energy and pitch angle distributions. In particular, Wood & Neukirch (2005) pointed out that Harris-type RCSs cannot yield power-law final kinetic distributions, while such distributions are the natural outcome of simulations of the acceleration process within X-type points (Wood & Neukirch 2005; Zharkova & Gordovskyy 2005). This remark notwithstanding, we shall argue below that the X-ray spectra emitted by the accelerated particles in a thick target model of radiation are, anyway, broader than their kinetic energy distributions, and that these spectra approach power laws even in the case of particles accelerated by Harris-type RCSs.

In the present work we perform numerical simulations of the acceleration of particles (electrons and protons) within single or multiple current sheets. In the case of flares, acceleration by a

*E-mail: cgontik@academyofathens.gr (CG); anastasi@space.noa.gr (AA); cefthim@academyofathens.gr (CE)

monolithic, large-scale, current sheet should be considered as a scenario of rather theoretical interest, which however helps setting up a number of basic formulae that are helpful in subsequent studies of more realistic scenario. A longstanding scenario regarding energy release in flares is the existence of *multiple dissipation sites* (Parker 1988). The assumption of fragmentation of the energy release in space and time during solar flares seems to be justified by several observations (e.g. Benz 1985; Dennis 1985; Benz & Aschwanden 1992; Crosby, Aschwanden & Dennis 1993; Aschwanden et al. 1995; Crosby et al. 1998; Krucker & Benz 1998; Aschwanden et al. 2000) indicating that the energy dissipation may occur in multiple and stochastically evolving current sheet configurations that coexist inside an active region. Past efforts to model this process numerically (Anastasiadis & Vlahos 1991, 1994; Anastasiadis, Vlahos & Georgoulis 1997; Anastasiadis et al. 2004; Vlahos, Isliker & Lepreti 2004) have clarified that several physical factors affect the efficiency of the acceleration process. A key factor is the dependence of the particles' *acceleration length* on the physical parameters of reconnection (e.g. strengths of the magnetic and electric fields and RCS thickness). In the present work, we compare the specific predictions for the acceleration length that were derived in our previous analytical studies with the results of simulations in which a large number of particles' orbits are integrated numerically.

We assume that the particles (electrons or protons) have initial velocities forming a Maxwellian distribution at coronal temperature 2×10^6 K. Such a distribution is used as generator of initial velocities for the orbits of a Monte Carlo sample of particles. The particles' orbits through RCSs are then integrated numerically. Entry pitch angles of the particles to an RCS are randomized in order to simulate a random distribution of the orientations of the RCSs encountered by the particles within a large active volume. Computations include the evolution of the particles' kinetic and pitch angle distributions, as well as the distribution of the times of escape of each particle from a sheet.

The paper is organized as follows. The basic RCS model, choice of units and computational scheme are presented in Section 2. Section 3 gives a comparison of numerical simulations with the analytical solutions given in Efthymiopoulos et al. (2005) and Gontikakis et al. (2006) for one encounter event. Section 4 deals with multiple interactions of the particles with a number of current sheets modelling a highly complex magnetic field configuration. Section 5 gives the computation of X-ray spectra produced by the accelerated electrons on the assumption of a thick target approximation. Finally, Section 6 summarizes the basic conclusions of the present study.

2 RCS MODEL AND COMPUTATION SET-UP

We consider the Harris-type model of Litvinenko & Somov (1993) to represent one local current sheet within an active region. The magnetic and electric fields inside one sheet of half-thickness a are given in equation (1):

$$\begin{aligned} E &= (0, 0, E), \\ B &= (-y/a, \xi_{\perp}, \xi_{\parallel})B_0 \quad \text{for } |y| \leq a. \end{aligned} \quad (1)$$

The edges of the current sheet are at $y = \pm a$. The magnetic field is normalized in units of B_0 , the value of the main reconnecting component at the edges. The magnetic field has two components, parallel and perpendicular to the current sheet plane, called the 'longitudinal' (ξ_{\parallel}) and 'vertical' (ξ_{\perp}) component, respectively. The existence of a longitudinal magnetic field can be justified in either a resistive magnetohydrodynamic context (Somov 1992; Litvinenko

& Craig 1999; Craig & Litvinenko 2002), or a purely collisionless regime (e.g. Horiuchi & Sato 1997). In particular, it has been argued (Litvinenko 1996) that the existence of a longitudinal field is necessary in order to explain electron acceleration by direct electric fields, since the Speiser orbits for electrons result in very small acceleration lengths. Indeed, in the limit $\xi_{\parallel} \rightarrow 1$ one finds $l_{\text{acc}}/a \sim \xi_{\parallel}/\xi_{\perp}$ (independent of E) which is much higher than the Speiser limit $l_{\text{acc}}/a \sim \epsilon/\xi_{\perp}^2$, with $\epsilon = Em/(aB_0^2 e)$ (m and e are the particle's mass and charge).

The equations of motion for a particle can be cast in a Hamiltonian form which is convenient in all subsequent calculations. In Efthymiopoulos et al. (2005) the initial Hamiltonian function, of three degrees of freedom, is reduced to a two degrees of freedom Hamiltonian by a 'momentum mapping' (Arnold & Novikov 2000). The final Hamiltonian reads

$$H = \frac{1}{2}p_y^2 + \frac{1}{2}\left(c_4 + \frac{1}{2}y^2\right)^2 + \frac{1}{2}(I_2 - \xi_{\perp}z + \xi_{\parallel}y)^2 - \epsilon z \quad (2)$$

with Darboux pairs (y, p_y) , (z, c_4) . The canonical momenta are mapped to velocities via $p_y = \dot{y}$, $c_4 = \dot{z} - \frac{1}{2}y^2$. I_2 is an integral of motion yielding the velocity of the x -component of motion (missing in equation 2), namely,

$$I_2 = \dot{x} - \xi_{\parallel}y + \xi_{\perp}z. \quad (3)$$

The above Hamiltonian describes the motions of positively charged particles. In the case of electrons we use the same equations of motion and then reverse the sense of the y - and z -axes, namely, $y_{\text{el}}(t) = -y(t)$, $z_{\text{el}}(t) = -z(t)$.

The choice of units is described in detail in Gontikakis et al. (2006, section 2). A typical value of the main magnetic field is $B_0 = 100$ G. A super-Dreicer electric field E of 100 V m^{-1} corresponds to $\epsilon = 10^{-5}$ for electrons and $\epsilon = (m_p/m_e) \times 10^5 \simeq 1.8 \times 10^{-2}$ for protons. In the dimensionless form of equation (2) the RCS half-thickness a is the unit of length, the inverse gyrofrequency $\omega_B^{-1} = m/qB_0$ is the unit of time ($\simeq 6 \times 10^{-10}$ s for electrons and 10^{-6} s for protons). We take a range of possible values of the dimensionless magnetic and electric field parameters, namely: $\xi_{\parallel} \in [0, 1]$, $\xi_{\perp} \in [10^{-3}, 10^{-2}]$, $\epsilon \in [10^{-5}, 10^{-4}]$.

We consider injections of particles into a current sheet with a Maxwell-Boltzmann velocity distribution corresponding to coronal temperature $T = 2 \times 10^6$ K. This is used to obtain a sample of initial velocity moduli for 10 000 particles per simulation. Particle injections are made at three different positions along the y -axis, that is, from the edges ($y = \pm 0.9$) or from the central plane. The choice $|y| = 0.9$, that is, slightly inside the sheet's formal edge, is dictated by the fact that the mean thermal velocity of the particles is typically larger than the drift velocity ($v_{\text{drift}} = \epsilon$) by one or more orders of magnitude, so that, when $|y| = 1$ is a sharp edge (as in equation 1), injection at that point ($|y| = 1$) would result in the particles always exiting the sheet after half a gyrocycle. The physical motivation behind the third choice, $y = 0$, is discussed in Gontikakis et al. (2006).

Initial particle velocities are distributed isotropically in the half-hemisphere of velocity space pointing towards the sheet, for injections at the edges, or the full sphere for injections at the central plane. This corresponds to a broad initial pitch angle distribution with a maximum at $\theta \simeq 90^\circ$. Since the equations of motion are symmetric with respect to translations in the z -axis we may always set the initial value of z equal to $z = 0$ without loss of generality. The initial values of y , z , \dot{x} are then used to determine the value of I_2 (equation 3) used in the integration of each particle. This is done by solving numerically Hamilton's equations of motion, derived by (2),

separately for each particle, that is, by assuming that the motion of each particle is not influenced by the motions of the other particles.

The numerical integration of the particles orbits is performed up to 10^5 time-steps corresponding to a total time $50 \mu\text{s}$ for electrons and to 0.1 s for protons. When a particle reaches $y = \pm 1$ it is considered as escaping the current sheet and the integration moves to the next particle. The stored output data are the kinetic energy, pitch angle, time of escape as well as the side of escape ($y = 1$ or -1) of each particle. In the simulations of multiple particle–RCS encounters, the output velocities of the particles after interacting with one RCS are used to specify the moduli of input velocities of the same particles into the next RCS.

3 SINGLE ENCOUNTERS

In the present section we examine in detail one step of the stochastic acceleration process, namely the interaction of the particles with a single current sheet. Some characteristics of the final distributions,

after the interaction, are common for both electrons and protons: (i) for most particles the kinetic energy gain is restricted in a relatively small energy range and (ii) final pitch angle distributions are narrower than the initial distributions. Both phenomena depend also somewhat on the choice of the RCS field values. A more detailed description of the experiments is given in the sequel, separately for electrons and protons.

3.1 Electrons

In the numerical experiments of electrons interacting with a single RCS, the electron energy distributions after the interaction are, in general, shifted towards higher values of the kinetic energy compared to the initial thermal distribution (Fig. 1). The amount of the shift reflects the efficiency of the RCS as accelerator. The mean thermal kinetic energy at temperature $2 \times 10^6 \text{ K}$ is 89 eV . In the numerical realization of the initial distribution by a finite number of particles ($N_{\text{particles}} = 10\,000$), there is a resolution limit reached at an

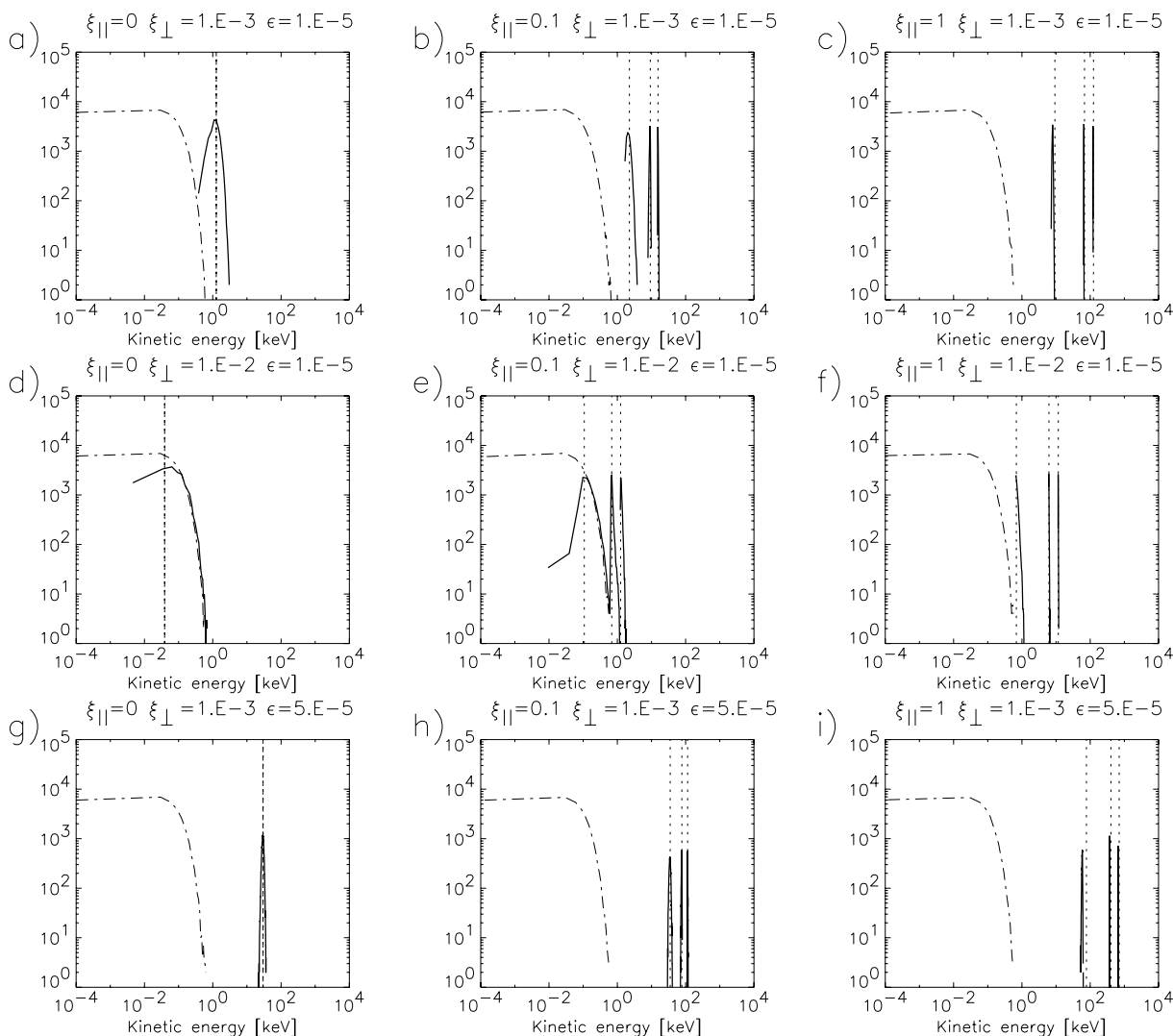


Figure 1. Electron kinetic energy distributions before (dot–dashed) and after (solid) the interaction with a single Harris-type RCS with parameters: (a) $\xi_{\parallel} = 0$, $\xi_{\perp} = 10^{-3}$, $\epsilon = 10^{-5}$; (b) $\xi_{\parallel} = 0.1$, $\xi_{\perp} = 10^{-3}$, $\epsilon = 10^{-5}$; (c) $\xi_{\parallel} = 1$, $\xi_{\perp} = 10^{-3}$, $\epsilon = 10^{-5}$; (d) $\xi_{\parallel} = 0$, $\xi_{\perp} = 10^{-2}$, $\epsilon = 10^{-5}$; (e) $\xi_{\parallel} = 0.1$, $\xi_{\perp} = 10^{-2}$, $\epsilon = 10^{-5}$; (f) $\xi_{\parallel} = 1$, $\xi_{\perp} = 10^{-2}$, $\epsilon = 10^{-5}$; (g) $\xi_{\parallel} = 0$, $\xi_{\perp} = 10^{-3}$, $\epsilon = 5 \times 10^{-5}$; (h) $\xi_{\parallel} = 0.1$, $\xi_{\perp} = 10^{-3}$, $\epsilon = 5 \times 10^{-5}$; (i) $\xi_{\parallel} = 1$, $\xi_{\perp} = 10^{-3}$, $\epsilon = 5 \times 10^{-5}$. In each simulation, three sets of 10 000 particles are injected at the initial positions $x = z = 0$ and $y = 0.9, 0$ or -0.9 . Vertical dotted lines correspond to an analytical estimate of the kinetic energy gain for the three different injection points.

energy 6.2 keV, after which the Maxwellian distribution is poorly sampled and the numerical distribution exhibits an abrupt cut-off.

The dispersion of kinetic energies in the final distributions of all experiments is of the same order of magnitude as in the initial thermal distribution. However, we find that the dispersion decreases somewhat as the value of the longitudinal magnetic field ξ_{\parallel} increases. This is in agreement with previous results of Wood & Neukirch (2005, their fig. 9) and Zharkova & Gordovskyy (2004), who explored numerically distributions similar to ours in the limit of a strong longitudinal field ($\xi_{\parallel} \rightarrow 1$).

For $\xi_{\parallel} \neq 0$, the kinetic energy gain depends on the injection position ($y = \pm 0.9$ or 0). As a rule, electrons injected at the lower edge ($y = 0.9$) acquire larger amounts of kinetic energies than those injected from the centre ($y = 0$) or upper edge ($y = -0.9$). As a result, when all injection positions are taken into account, the final distribution often appears to have three well distinct peaks (Fig. 1, except for the panels a, d, g). The energy values at which the peaks appear can be given by an approximate analytical theory. The maximum kinetic energy gain for one particle can be expressed as a function of the field parameters, the position of injection into the sheet and the initial energy of the particle. The final formula (Efthymiopoulos et al. 2005; Gontikakis et al. 2006) reads

$$E_{\max}(E_0, \dot{x}_0, y_0, y_{\text{out}}; \xi_{\parallel}, \xi_{\perp}, \epsilon) = \frac{\epsilon}{\xi_{\perp}^2} (\xi_{\perp} I_2 + \xi_{\parallel} \xi_{\perp} y_{\text{out}} \epsilon + \epsilon + \sqrt{2\xi_{\perp} I_2 \epsilon + 2\xi_{\parallel} \xi_{\perp} y_{\text{out}} \epsilon + \epsilon^2 + 2\xi_{\perp}^2 E_0}), \quad (4)$$

where E_0 is the initial kinetic energy of a particle injected at $y = y_0$, the value of I_2 is set equal to $I_2 = \dot{x}_0 - \xi_{\parallel} y_0$, and the exit of the particle is through the edge $y = y_{\text{out}}$. We may compute an average value of E_{\max} for a thermal distribution of particles by setting $E_0 = \langle E_0 \rangle = 89$ eV and $\dot{x}_0 = \langle \dot{x}_0 \rangle = 0$ in the above formulae. We also set $y_{\text{out}} = 1$ since the maximum of the acceleration length always occurs when the exit of electrons is from the lower edge ($y_{\text{out}} = 1$). The analytical predictions based on the above assumptions are shown as dashed vertical lines in each panel of Fig. 1. The agreement with the peaks of the numerical distributions is always good and it allows us to conclude that most electrons acquire kinetic energies which are close to the maximum value allowed by equation (4). Only for very strong values of the longitudinal field ($\xi_{\parallel} = 1$ in Figs 1c, f and i) the electrons end up with an energy which is a fraction (of the order of unity) of the analytically predicted value. In fact, it can be demon-

strated that the motion of most particles in this limit is restricted on invariant surfaces (invariant tori) that correspond to the preservation of an adiabatic invariant Efthymiopoulos et al. (2005). This results in the particles leaving the sheet at a point corresponding to the intersection of an invariant surface with the sheet's edge, yielding a value of the kinetic energy upon exit which can be below the upper limit of equation (4). On the other hand, when ξ_{\parallel} is relatively small ($\xi_{\parallel} < 0.1$), the motions of most electrons within the sheet are chaotic, and the electrons acquire kinetic energies which are, in general, very close to the maximum limit given by equation (4).

When $\xi_{\parallel} \neq 0$, equations (3) and (4) imply that the maximum kinetic energy depends on the point of injection y_0 ; as y_0 decreases, I_2 and E_{\max} increase. Thus, the kinetic energy gain is maximum for electrons injected at the upper edge ($y_0 = -0.9$). From the physical point of view, these are electrons traversing the sheet all across its width, thus they ‘feel’ the electric field for times larger than the electrons injected at the lower edge $y_0 = 0.9$. Furthermore, as the value of ξ_{\perp} decreases, the kinetic energy gain increases due to the $1/\xi_{\perp}^2$ factor in equation (4). This is clearly seen in Figs 1(d)–(f). In fact, in the limit $\xi_{\perp} \rightarrow 0$ the electrons follow Speiser orbits for which $E_{\max} \sim \epsilon^2/\xi_{\perp}^2$.

The pitch angle distributions of electrons interacting with an RCS become steeper for higher values of ξ_{\parallel} (Fig. 2a). When $\xi_{\parallel} = 0$ the pitch angles of electrons escaping from the lower edge of the current sheet reach values up to 60° , while in the case of escape from the upper edge the pitch angles are larger than 90° . Due to the opposite orientations of the magnetic field at the RCS edges, the final distributions of the pitch angles are rather symmetric with respect to the value of 90° (Fig. 2a, where we also show the initial pitch angle distribution (dot-dashed line) resulting from an isotropic distribution of velocities in a hemisphere of velocity space pointing towards the sheet). A non-zero longitudinal magnetic field introduces a preferential edge of the sheet (lower for electrons, upper for protons in the orientation of the fields as in equation 1) from which the majority of particles escape. This phenomenon can also be explained theoretically (Efthymiopoulos et al. 2005). In particular, for electrons with energy E_0 there is a threshold value of $\xi_{\parallel} = (\epsilon^2 + 2E_0\xi_{\perp}^2)/2\xi_{\perp}\epsilon$ above which escapes are possible exclusively from the lower edge $y_{\text{out}} = 1$.

Finally, the time needed for electrons to escape from the RCS depends also mainly on ξ_{\parallel} and on the injection point (Fig. 3a). We

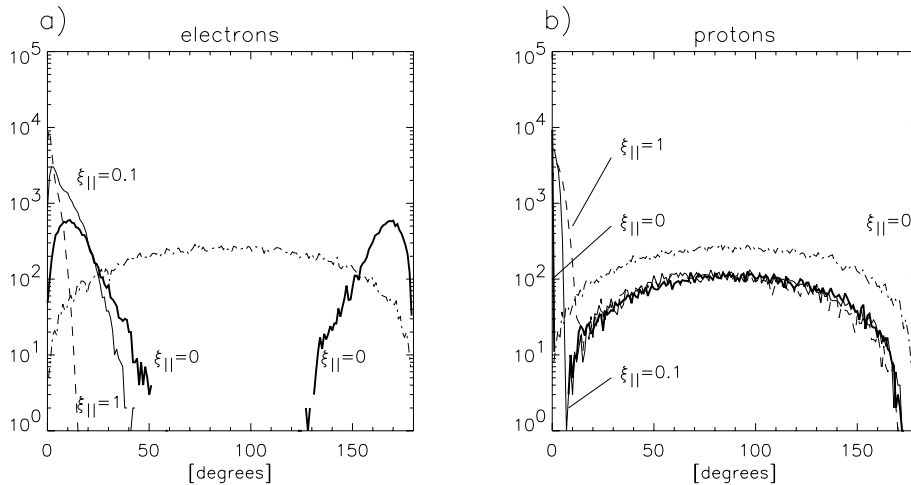


Figure 2. Initial (dot-dashed) and final (solid) pitch angle distributions for the same numerical simulations as in (a) Figs 1(a)–(c) for electrons, and (b) Figs 4(a)–(c) for protons. In the case of electrons, larger values of ξ_{\parallel} correspond to narrower final pitch angle distributions, while the opposite is true in the case of protons.

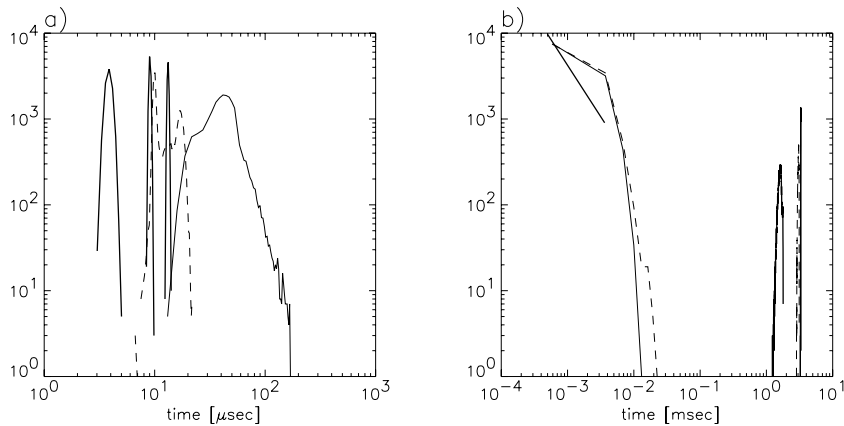


Figure 3. Distribution of the times of escape of (a) electrons and (b) protons from a single RCS. The model parameters are the same as those of Fig. 2(a) for electrons and Fig. 2(b) for protons. Thick lines (the three-peaked curve in panel a and the one-peaked curve at 1–2 ms in panel b) correspond to $\xi_{\parallel} = 1$ dashed lines to $\xi_{\parallel} = 0.1$ and thin lines to $\xi_{\parallel} = 0$.

find that the time of escape decreases on average as the value of ξ_{\parallel} increases. This leads to the effect that while the time particles spend within the RCS decreases the amount of kinetic energy that they gain increases on average.

3.2 Protons

In the numerical simulations for protons we adopt the same values of the dimensionless magnetic field parameters as for electrons, and rescale the value of the dimensionless electric field by a factor m_p/m_e (see Section 2).

The kinetic energy distributions before and after the interaction of the protons with an RCS are shown in Fig. 4. Clearly, the main difference with respect to the corresponding electron distributions is that an important fraction of protons are not accelerated. This happens mainly in the case of injections from the edges. The typical orbit for protons entering the sheet at the edges is to perform a single gyration and then escape without any energy gain. For some model parameters up to half of the protons retain the initial thermal distribution (Fig. 4). Thus the final distributions for protons typically show a thermal branch of non-accelerated protons and a branch of accelerated protons, shifted with respect to the initial thermal distribution.

The sets of initial conditions leading to the non-accelerated or the accelerated component form two well-separated domains in velocity space. Fig. 5 shows the initial conditions in velocity space for particles injected at the upper edge ($y = 0.9$). We find that the initial velocities of accelerated protons are always restricted in a domain defined by the inequalities $V_z > -V_x$ and $V_y > V_{th}$, with a threshold value determined numerically as $V_{th} \simeq 0.5$. In the case of non-accelerated protons, we still find a threshold $V_y < V_{th}$ with $V_{th} \simeq 0.5$ whenever $V_z > -V_x$, or $V_y > V_{th}$ whenever $V_z < -V_x$ for the majority of initial conditions. However, the initial conditions of a small fraction of non-accelerated protons lie within the domain of initial conditions of the accelerated protons, so that there is a small overlap of the two domains.

Unlike the case of electrons, the final kinetic energy distributions of protons are not very sensitive to the value of the longitudinal magnetic field ξ_{\parallel} . When $\xi_{\parallel} \neq 0$, accelerated protons escape preferentially from one edge of the sheet, while non-accelerated protons escape equally probably from both sides of the sheet. Final kinetic energy distributions are centred at mean values of the order of

$10 \sim 100$ MeV, with narrow dispersions of the order of 100 eV, that is, the same order as in the initial thermal distribution. These results can be explained again on the basis of equation (4). The main point to note is the increased value of the dimensionless electric field ϵ . Physically, this implies that the character of motion inside the sheet is determined by the electric rather than the magnetic field. This is because the typical gyroradii for protons in thermal motion are of the same order of magnitude as the RCS half-width so that the Speiser type of orbits becomes irrelevant for most protons. On the other hand, equation (4) is still valid so that the peaks of the numerical distribution are again well represented by this formula (Fig. 4).

The final pitch angle distributions of protons (Fig. 2b) are typically separated also in two components. In the case of non-accelerated protons, the initial and final pitch angle distributions have roughly the same form. On the contrary, in the case of accelerated protons the final pitch angle distribution is a function peaked close to 0° (when $\xi_{\parallel} = 0$ a second peak appears also at 180° corresponding to protons escaping the sheet from the lower edge $y = -1$). Another difference with respect to electrons is that the pitch angle distributions of accelerated protons become broader as the value of ξ_{\parallel} increases (see also Zhu & Parks 1993). Finally, the distribution of the times of escape of protons clearly shows a separation between the non-accelerated protons, for which the mean time of escape is of the order of the gyroperiod at the edge of the sheet, and the accelerated protons that spend about $10^3 - 10^4$ gyroperiods within the sheet before they escape (Fig. 3b).

4 MULTIPLE PARTICLE-RCS ENCOUNTERS MODELLED AS A STOCHASTIC PROCESS

The scenario of particle acceleration via a monolithic current sheet may be of relevance only in the case of the largest (eruptive) flares. In a more realistic scenario, which is applicable particularly in the case of smaller (compact) flares, it is necessary to consider complex magnetic topologies within which multiple current sheets are formed. In this section we present simulations of a stochastic acceleration process in such a complex magnetic topology. In particular, we consider an initially thermal distribution of particles that have consecutive encounters with more than one current sheets. Each encounter is viewed as an impulsive event that is well separated in time from the next encounter. This is because the characteristic times of escape of particles from one sheet are smaller by orders of

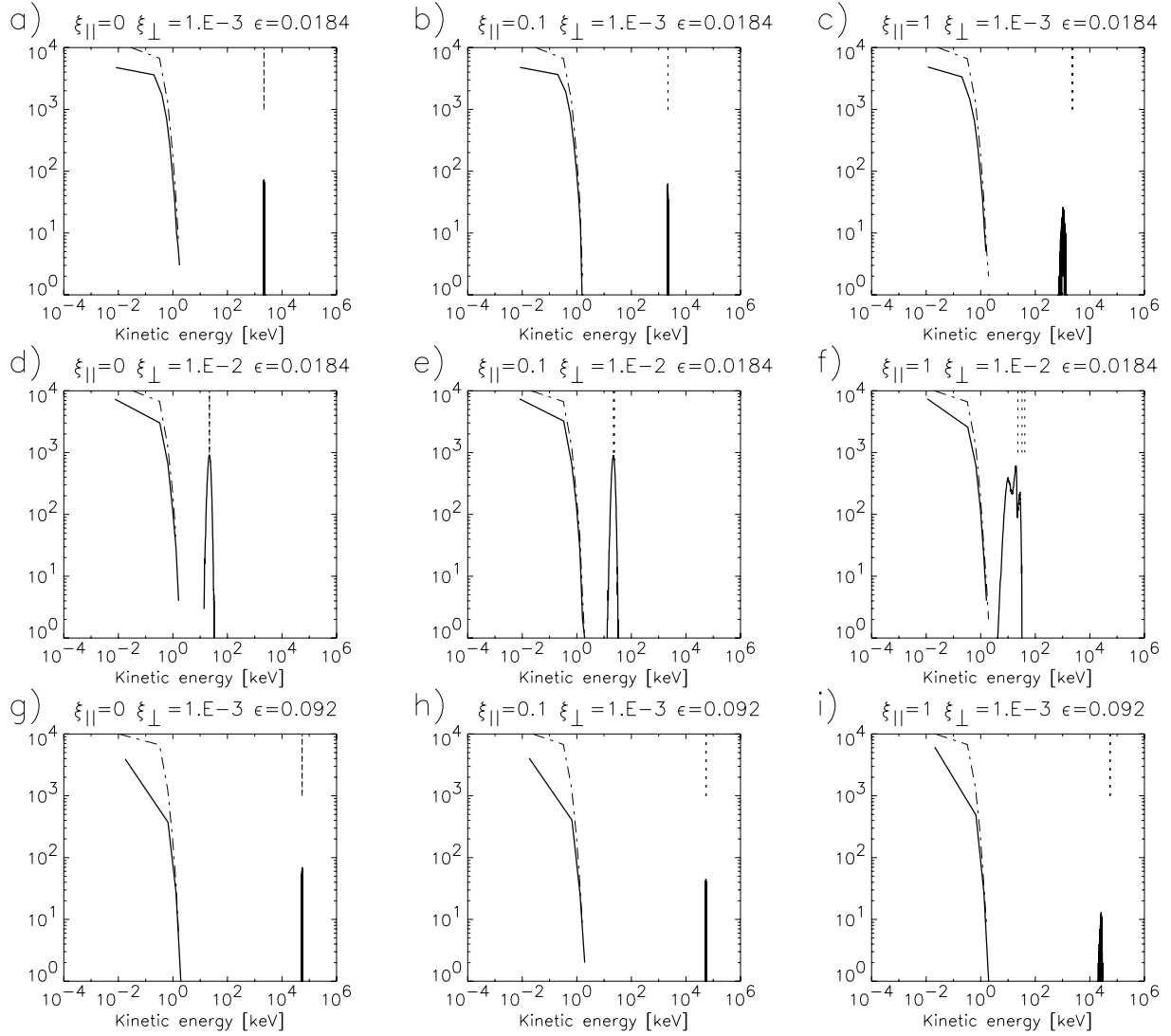


Figure 4. As in Fig. 1, but for the proton kinetic energy distributions. The dimensionless electric field parameter ϵ is rescaled with respect to the values given in Fig. 1 by a factor of $m_p/m_e = 1.84 \times 10^3$.

magnitude from the dynamical time-scale of evolution of the magnetic field configuration.

After one particle–RCS encounter is accomplished, the particles are assumed to follow a random walk path in configuration space that leads them to a second encounter with a different RCS in a random location within the same active region. The process may then be repeated ad infinitum. In every consecutive step the dimensionless field parameters (ξ_{\perp} , ξ_{\parallel} , ϵ) are assigned random values from a homogeneous distribution in the intervals $0 \leq \xi_{\parallel} \leq 1$, $10^{-3} \leq \xi_{\perp} \leq 10^{-2}$ and $5 \times 10^{-6} \leq \epsilon \leq 3 \times 10^{-5}$ for electrons or $3.7 \times 10^{-3} \leq \epsilon \leq 5.5 \times 10^{-2}$ for protons. We furthermore randomize the injection pitch angle of each particle. We thus allow particles to enter the new sheet isotropically from either edge (but not from the centre).

Figs 6 and 7 show an example of the time evolution of the kinetic energy distribution after 10 consecutive particle–RCS encounters in the case of electrons and protons, respectively. In both figures, panel (a) shows the initial thermal distribution. As shown in Fig. 6(b), the electron kinetic energy distribution after the interaction with the first current sheet presents two peaks that correspond to the two entry points at $y = 0.9$ and $y = -0.9$ (Section 3.1). In the next step, each peak is split in two new peaks, etc. Thus, after N steps the number of

peaks is of the order of $O(2^N)$. If we assign a localized (say Gaussian) distribution around each peak, as N increases the local distributions have a significant overlap. This results in that the total distribution, which is the sum of all the local distributions, tends to become a broad smooth function (panels f–k). In the case of electrons, the asymptotic decay of this function for large energies is well fitted by an exponential law, while in the case of protons it is reasonably well fitted both by an exponential or power law.

The most relevant result coming out of these simulations is that the kinetic energy distribution of the particles tends to converge to a final form after a relatively small number of interactions (of the order of 10). For example, Fig. 6(l) shows the superposition of the kinetic energy distributions corresponding to the three last steps of the simulation for electrons (panels i, j, k of the same figure). Clearly, there is no significant variation of the distribution in the last three steps. This also implies that there is an upper kinetic energy limit for electrons which is reached at the tail of the final distribution at an energy of the order of $E \simeq 100$ keV.

We may model the above acceleration process as a discrete stochastic process describing the generation of local distributions around multiple peaks during the consecutive particle–RCS

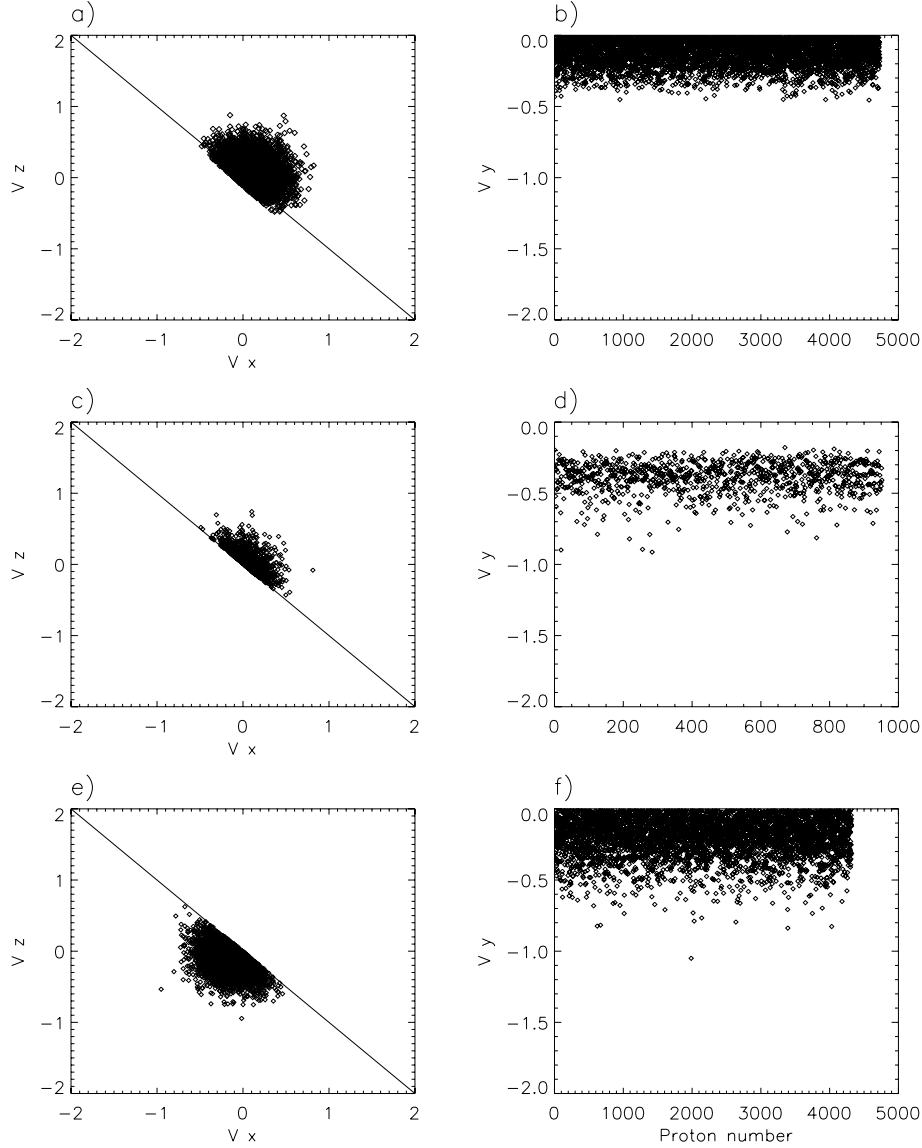


Figure 5. Separation of the initial conditions in velocity space for accelerated or non-accelerated protons, when $\xi_{\parallel} = 1$, $\xi_{\perp} = 10^{-3}$, $\epsilon = 0.018$ and $y_0 = 0.9$. Accelerated protons have initial velocities (a) $v_z > -v_x$ and (b) $v_y > -0.5$. Non-accelerated protons have velocities satisfying either (c) $v_z > -v_x$ and (d) $v_y < -0.5$, or (e) $v_z < -v_x$ and (f) $v_y > -0.5$.

interactions. Let

$$n_N(E) = \sum_{j=1}^{M_N} \frac{A}{\sqrt{2\pi}\sigma} \exp \left\{ -\frac{[E - E_j^{(N)}]^2}{2\sigma^2} \right\} \quad (5)$$

represent the kinetic energy distribution after N consecutive particle–RCS interactions, $N = 0, 1, 2, \dots$, that is, the total distribution is given as a sum of M_N local distributions with dispersion σ around the peaks $E_j^{(N)}$, $j = 1, 2, \dots, M_N$. We set $M_0 = 1$, that is, initially there is only one peak at the mean thermal energy $E_1^{(0)} = \langle E_{\text{th}} \rangle$. Each of the peaks $E_j^{(N)}$ produces new peaks according to the formula

$$E_k^{(N+1)} = C_f (E_j^{(N)} + E_{\max}(E_j^{(N)}, 0, -0.9, 1; \xi_{\parallel}^{(N+1)}, \xi_{\perp}^{(N+1)}, \epsilon^{(N+1)})) \quad (6)$$

and

$$E_{k'}^{(N+1)} = C_f (E_j^{(N)} + E_{\max}(E_j^{(N)}, 0, 0.9, 1; \xi_{\parallel}^{(N+1)}, \xi_{\perp}^{(N+1)}, \epsilon^{(N+1)})), \quad (7)$$

where E_{\max} is given by equation (4). The two peaks correspond to the particles entering the sheet from either the lower or upper edge ($y_0 = \pm 0.9$).

If the field parameters $\xi_{\parallel}^{(N+1)}$, $\xi_{\perp}^{(N+1)}$, $\epsilon^{(N+1)}$ are selected from a random sequence, then equations (6) and (7) define a stochastic process. In the actual calculation we use the same random sequence as in the successive snapshots of Fig. 6 so that a comparison of the resulting distributions is possible. There are two free parameters in the model, namely the dispersion σ of each local distribution around its peak and a coefficient C_f satisfying $0 \leq C_f \leq 1$. The meaning of C_f is that the particles belonging to a particular local distribution are assumed to acquire, on average, an energy equal to the constant factor C_f times their maximum possible energy after the interaction with an RCS with parameters $(\xi_{\parallel}^{(N+1)}, \xi_{\perp}^{(N+1)}, \epsilon^{(N+1)})$.

Fig. 8 shows the resulting energy distributions for electrons for $N = 8, 9, 10$ and a choice of parameters $\sigma = 2 \times 10^{-3}$ [in dimensionless units (corresponding to ~ 12 keV)], and $C_f = 0.5$. It is immediately observed that the final distribution obtained with this

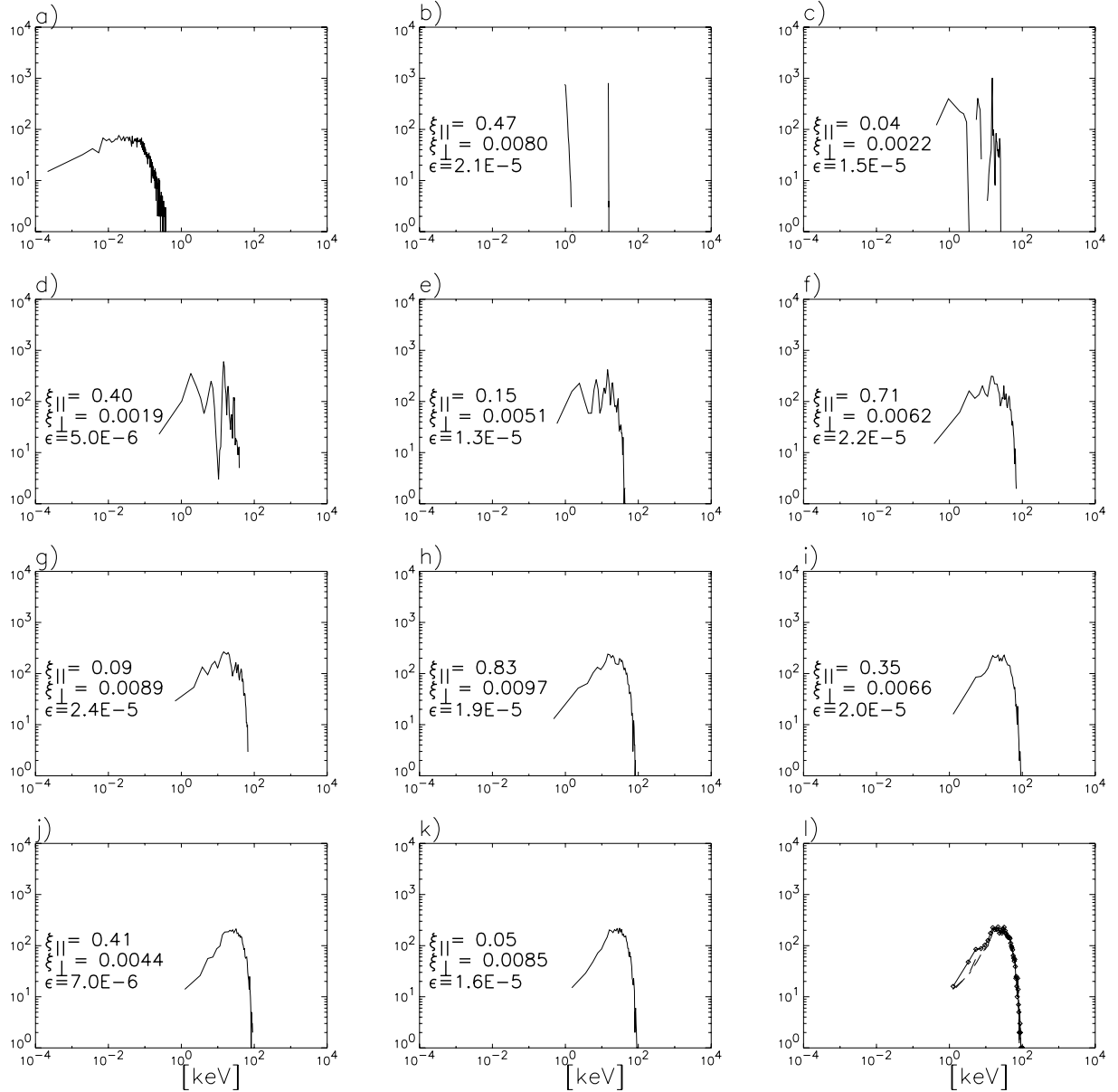


Figure 6. (a) The initial (thermal) energy distribution of electrons. (b–k) The form of the same distribution after consecutive interactions of the electron population with a number of current sheets. The RCS field parameters (ξ_{\parallel} , ξ_{\perp} , ϵ) of each event are written within the corresponding panel. (l) Superposition of the plots (i), (j) and (k).

simple stochastic model fits well the distribution obtained by the actual particles' simulation except in the region of very low energies (~ 1 keV). This is expected because we assumed a uniform value of σ throughout the entire range of energies, while, in reality, σ is an increasing function of the energy. At any rate, the fact that the three theoretical distributions for $N = 8, 9, 10$ are very similar indicates that a simple modelling of the acceleration as a discrete stochastic process allows one to recover the tendency of the energy distribution to reach a constant asymptotic limit as $N \rightarrow \infty$.

Similar phenomena are observed in the simulations for protons (Fig. 7). In this case, the initial splitting of the energy distribution is in a 'thermal' and an 'accelerated' component (panel b). As the protons interact with successive current sheets, the particles of both components gain kinetic energy. The merging of the various components results to a considerable broadening of the final distribution

(10^3 keV), which is five orders of magnitude larger than the broadening of the initial thermal distribution ($\sim 10^{-2}$ keV). Still, the main phenomenon is the convergence of the whole process towards a final distribution (panels i–l in Fig. 7). The convergence takes place when the protons reach energies of the order of $10 \sim 100$ MeV.

In order to understand the tendency of the energy distribution to reach an asymptotic limit, the key point is to note, through equation (4), that the efficiency of a single RCS as accelerator depends not only on the field parameters (ξ_{\perp} , ξ_{\parallel} , ϵ), but also on the *initial* energy E_0 of the particles being accelerated. It turns out that, as E_0 increases, the volume of the domain of parameter values (ξ_{\perp} , ξ_{\parallel} , ϵ) for which an RCS can still be an efficient accelerator decreases. This can be quantified with the help of Figs 9(a) and (b). Let w be the amplification factor of the maximum particle energy gain at one encounter event with respect to the initial energy E_0 , namely

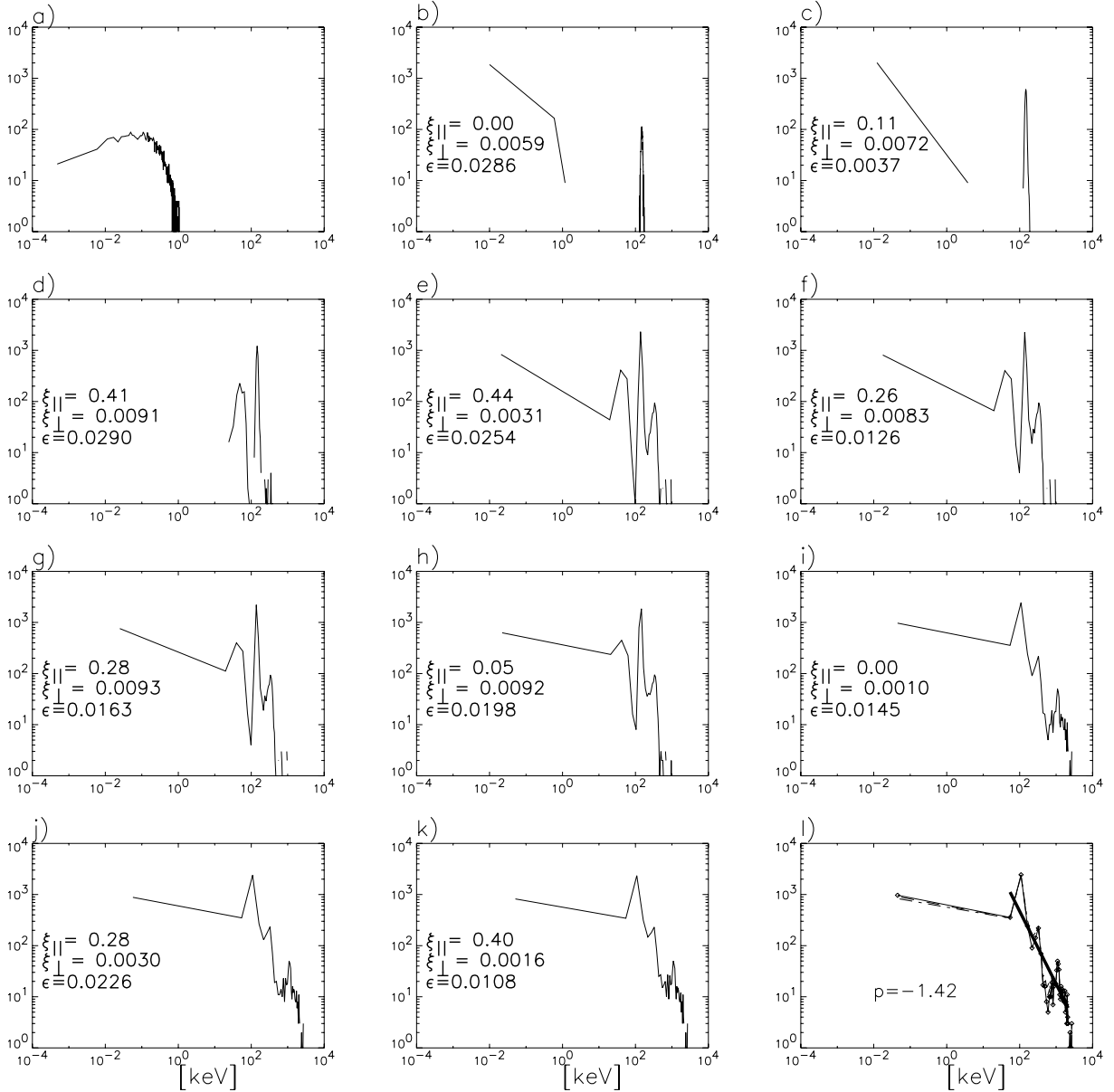


Figure 7. Same as in Fig. 6 but for protons. The thick line in (l) is a power-law fitting of the final distribution.

$E_{\max} = w E_0$. The ordinate in Fig. 9(a) (electrons) or (b) (protons) is the probability that a current sheet with parameters belonging to the range $0 \leq \xi_{\parallel} \leq 1$, $10^{-3} \leq \xi_{\perp} \leq 10^{-2}$, $5 \times 10^{-6} \leq \epsilon \leq 3 \times 10^{-5}$ for electrons and $3.7 \times 10^{-3} \leq \xi \leq 5.5 \times 10^{-2}$ for protons is an efficient accelerator, that is, E_{\max} given by equation (4) satisfies $E_{\max} \geq E_0$, as a function of the initial energy E_0 shown in the abscissa. The probability is calculated by dividing the above cubic volume of the parameter space in a $10 \times 10 \times 10$ cubic grid and calculating E_{\max} , for given E_0 , at all points of the grid. The five curves in each panel correspond to different values of w , namely, $w = 1, 0.5, 0.1, 0.01$ and 0 from left- to right-hand side. Thus $w = 1$ means that a particle doubles its initial energy while $w = 0$ means that the particle does not gain any energy at all.

When the particles' initial kinetic energy E_0 is small (say of the order of 1 keV or smaller), the probability for all five curves of each panel tends to the unity. This implies that an RCS with almost any combination of values (ξ_{\perp} , ξ_{\parallel} , ϵ) is an efficient particle accelerator.

However, as E_0 increases, say by the consecutive encounters of the particles with RCSs, the probability that one RCS is efficient accelerator decreases and it tends to zero as the energy E_0 tends to a limiting value. In the case of electrons, this value is about $E_{0,\text{lim}} = 210$ keV when $w = 1$, while it tends to a value $E_{0,\text{lim}} \rightarrow 425$ keV as $w \rightarrow 0$ (dashed line in Fig. 9a). This value represents the maximum kinetic energy that can be reached by an electron after any arbitrarily large number of consecutive interactions with RCSs in the above specified range of field parameters. In the case of protons, the corresponding limit is $E_{0,\text{lim}} = 40$ MeV (Fig. 9b). In fact, the tendency of the final distribution to converge to a constant asymptotic form is manifested when the energy distribution reaches values which are below the uppermost limit $E_{0,\text{lim}}$, although they are of the same order of magnitude. For example, the limiting distribution for electrons (Fig. 6l) corresponds to energies ~ 100 keV. As shown in Fig. 9(a), the probability that the particles meet an efficient RCS accelerator at this level of energy is only a few per cent, even when

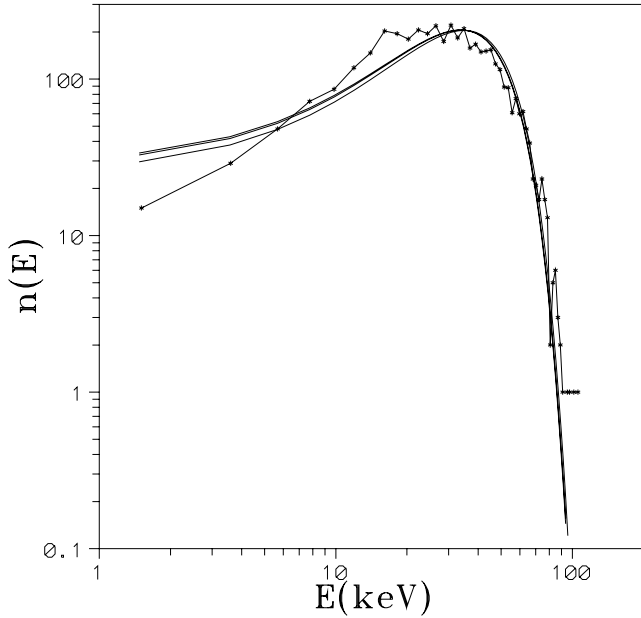


Figure 8. The electron kinetic energy distribution of Fig. 6(l) (dots) compared to three theoretical distributions derived by a simple stochastic model (equations 6 and 7) after $N = 8, 9$ or 10 particle–RCS interactions.

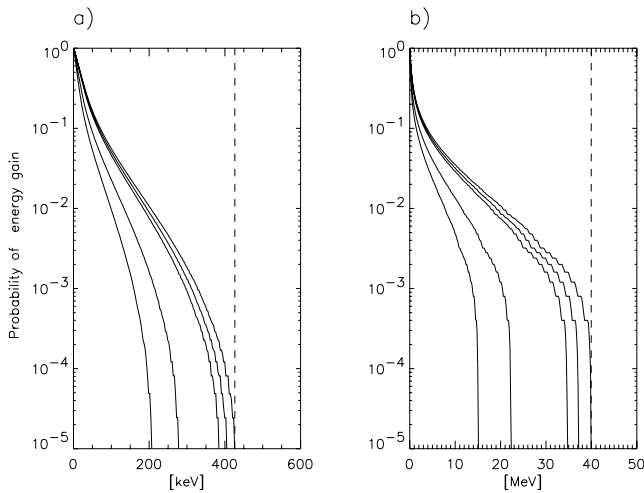


Figure 9. Probability for an electron (a) or a proton (b), with given initial kinetic energy E_0 to acquire an energy equal to $(1 + w)E_0$, where w takes the values 1, 0.5, 0.1, 0.01 and 0 (from left- to right-hand curve in each panel).

w is as high as $w = 1$, while this probability is below 1 per cent when a particle reaches energy ~ 200 keV. Similar probabilities are found for the protons (Fig. 9b) when the energy reaches values of the order of 2 MeV, that is, as in the final distributions of Fig. 7(l).

5 THEORETICAL X-RAY SPECTRA

A question of particular interest regards the expected form of the spectra of X-rays that are emitted when highly energetic particles, such as those resulting from the simulations of the previous sections, interact with a dense medium and radiate. Thick target radiation (Brown 1971; Vilmer, Trotter & Kane 1982; Anastasiadis et al. 2004) provides a basic model for such an interaction. In the thick target approach, the electrons, after escaping from the reconnection region,

have impacts with the chromosphere resulting in a loss of kinetic energy at very small times with no modification due to transport. The X-ray emission is produced by bremsstrahlung radiation. In the computation of the X-ray spectrum one starts with the number of photons of energy $h\nu$ emitted by an electron of initial energy E_0 :

$$\mu(h\nu, E) = \int_{E_0}^{h\nu} \sigma(h\nu, E) n_p v(E) \frac{dE}{dt}, \quad (8)$$

where $\sigma(h\nu, E)$ is the cross-section coefficient of the bremsstrahlung emission, n_p the density of the ambient plasma, $v(E)$ the electron's velocity and dE/dt the energy loss due to collisions. Then, the photon spectrum emitted by an electron distribution $F(E_0)$ in the range $E_0, E_0 + dE$ is given by the integral

$$I(h\nu) = \int_{h\nu}^{+\infty} F(E_0) \mu(h\nu, E_0) dE_0. \quad (9)$$

We implemented the above formulae in order to compute a theoretically expected X-ray spectrum for each of the electron kinetic energy distributions shown in the previous sections. The computations are meaningful only when a kinetic energy distribution has a significant contribution at energies above a threshold value 1.6 keV. On the other hand, when the maximal kinetic energy of a distribution is in the range of $\simeq 3$ keV (Figs 1d and e) the X-ray computation is not accurate.

Typical computed X-ray spectra corresponding to the kinetic energy distribution of the particles after the interaction with a single RCS, are shown in Figs 10(a)–(c). We find that the maximum photon energy corresponding to a particular kinetic energy distribution is lower but close to the maximal kinetic energy of this distribution. However, the main difference between the X-ray spectra and the distributions is that the X-ray spectra are broad and smooth functions of the energy, in contrast to the particles distributions which are sharply peaked. The smoothing is due to the fact that the X-ray spectrum involves an integral (equation 9) over the kinetic energy distribution that smooths out the sharp peaks of the latter. A typical X-ray spectrum shows a monotonic decrease with rising photon energy, up to a maximal cut-off value of the photon energy. The spectra can be partly represented by power laws $\propto E^{-p}$ up to the cut of energy. In the case of single RCS encounter the spectra are steep functions when the longitudinal field ξ_{\parallel} is small, while they become more shallow ($p \simeq 2$) as the longitudinal field tends to the value of the mean reconnecting component ($\xi_{\parallel} \rightarrow 1$). On the other hand, acceleration processes modelled by multiple particle–RCS interactions lead also to power-law spectra with ($p \simeq 2$) followed by a rather smooth decrease near the maximal photon energy (Fig. 10d). The spectra of Figs 10(c) and (d), have maximal photon energies of $\simeq 100$ keV. This makes them good candidates to compare with observations of non-thermal X-rays.

6 CONCLUSIONS AND DISCUSSION

In the present paper we studied the particle acceleration process and the resulting energy distributions of charged particles interacting with a single Harris-type RCS, and then with a complex magnetic topology consisting of multiple RCSs. The initial particle distribution is thermal, corresponding to a solar coronal temperature.

Our main conclusions are the following.

- (i) A Harris-type RCS with field values relevant to solar flares typically accelerates the entire ingoing thermal ensemble of electrons, while it accelerates only part of a thermal ensemble of protons (about 60–70 per cent).

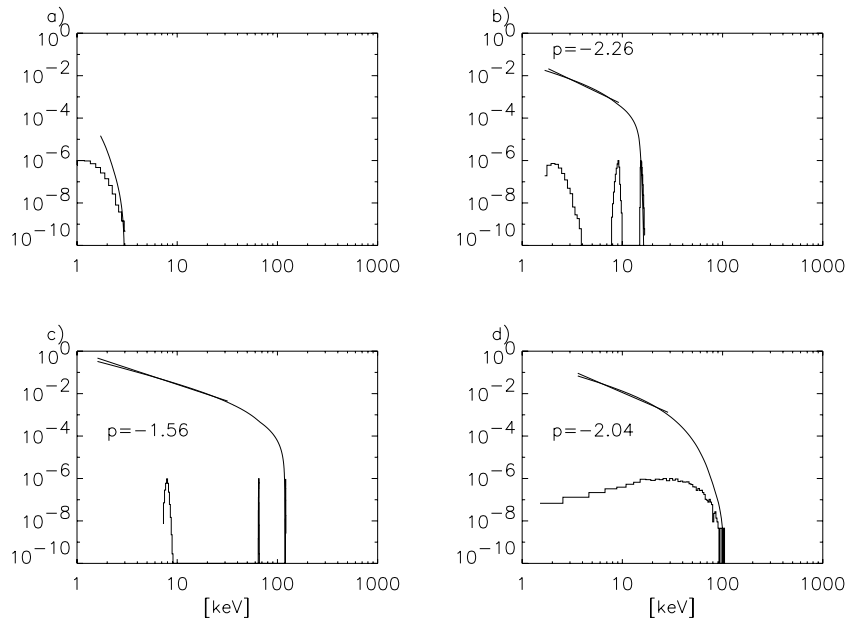


Figure 10. X-ray spectra (upper curves) compared to the electron kinetic energy distributions which produce them (lower curves) after a single particles–RCS interaction with $\xi_{\perp} = 10^{-3}$, $\epsilon = 10^{-5}$ and (a) $\xi_{\parallel} = 0$, (b) $\xi_{\parallel} = 0.1$ and (c) $\xi_{\parallel} = 1$. (d) Same as (a)–(c) in the simulation of multiple particle–RCS interactions for electrons.

(ii) The time spent by the particles within the RCS can be as large as 0.1 ms for electrons and a few ms for protons. This is still under the limit of the temporal resolution of present instruments. Furthermore, the kinetic energy gain decreases, on average, when the time of stay in the current sheet increases (see Fig. 3).

(iii) The pitch angle distributions of accelerated particles are typically sharply peaked at values corresponding to orientations almost parallel to the reconnecting magnetic field component. In the case of electrons the peak becomes narrower as the longitudinal magnetic field ξ_{\parallel} increases. The opposite is observed in the case of protons.

(iv) In single RCS encounter events, the final kinetic energy distribution is typically narrow and multi-peaked. However, if multiple events take place, the final distribution broadens and the peaks disappear. The dispersion of the final distribution is typically larger by more than two orders of magnitude than in the initial thermal distribution. The acceleration process can be modelled as a discrete stochastic process incorporating the basic laws of particle acceleration found in our previous works (Efthymiopoulos et al. 2005; Gontikakis et al. 2006).

(v) The kinetic energy distributions of both electrons and protons tend to acquire a limiting final form after a relatively small number of particle–RCS interactions (of the order of 10). This tendency can be explained theoretically in terms of the probability of an RCS to be efficient accelerator, as function of the input energy of the particles E_0 , when the field parameter of the RCSs take values restricted in a given volume of the parameter space. This probability decreases as E_0 increases. This means also that there is an upper limit in the ultimate energy that can be gained by the particles in a multiple RCS encounter scenario. In solar flare conditions, this is of the order of $10^2 \sim 10^3$ keV for electrons, or $10 \sim 100$ MeV for protons.

(vi) The X-ray spectra computed from the energy distributions of accelerated electrons, via a thick target modelling, have maximal photon energies around 100 keV and they compare well with observations. In the case of a single particle–RCS interaction, the X-ray spectra have logarithmic slopes of the order of $p = -2$ with a tendency of the slope to decrease as the longitudinal field increases.

In the case of multiple encounter events the average slope is also around -2 . The X-ray spectra exhibit cut-offs at energies ~ 100 keV. This is in agreement with observations of flat X-ray spectra in the literature indicating similar energy cut-offs (e.g. Nitta, Dennis & Kiplinger 1990).

A number of works in the literature have addressed the questions of particle acceleration and of the energy distributions produced by ensembles of test particles accelerated within various types of reconnection topologies (Bulanov 1980; Tajima et al. 1987; Martens 1988; Burkhart, Drake & Chen 1990; Martens & Young 1990; Deeg, Borovsky & Duric 1991; Bruhwiler & Zweibel 1992; Moses, Finn & Ling 1993; Kliem 1994; Litvinenko 1996; Fletcher & Petkaki 1997; Petkaki & MacKinnon 1997; Vekstein & Browning 1997; Mori, Sakai & Zhao 1998; Browning & Vekstein 2001; Craig & Litvinenko 2002; Heerikhuisen, Litvinenko & Craig 2002; Hamilton et al. 2003; Zharkova & Gordovskyy 2004; Dalla & Browning 2005; Hamilton et al. 2005; Wood & Neukirch 2005; Zharkova & Gordovskyy 2005; Hannah & Fletcher 2006). Thus some general conclusions can be drawn as regards how do our results compare with previous results from the literature and what is to be learned from the simulations described in the present study.

It has shown that the tails of the final energy distributions are well fitted either by exponential laws (e.g. Bulanov 1980; Deeg et al. 1991; Bruhwiler & Zweibel 1992), or power laws (e.g. Vekstein & Browning 1997; Mori et al. 1998; Browning & Vekstein 2001; Dalla & Browning 2005; Hannah & Fletcher 2006), almost independently of the details of the initial conditions of the particles' distribution, as long as the magnetic field topology is hyperbolic. On the other hand, the final distributions of particles accelerated in Harris-type RCSs are almost monoenergetic (Zharkova & Gordovskyy 2004; Wood & Neukirch 2005, and Section 3 above). However, as exemplified in Section 4, the exponential or power laws arise, even in that case, when one considers a stochastic process involving many Harris-type RCSs. This fact suggests that a suitable basis for a theoretical modelling of the particle acceleration process in complex

reconnection topologies is that of a *stochastic process* leading to a constant asymptotic limit, that is, a constant final energy distribution after a number of iterations of the process. This point of view is also supported by the evidence that far from the adiabatic limit, that is, close to X-points, islands or other critical topologies, the typical particles' orbits are *chaotic* (e.g. Büchner & Zelenyi 1991; Litvinenko & Somov 1993; Zhu & Parks 1993; Kliem 1994; Hannah, Fletcher & Hendry 2002; Dalla & Browning 2005; Efthymiopoulos et al. 2005; Gontikakis et al. 2006; Hannah & Fletcher 2006). Namely, our numerical evidence suggests that, as long as an ensemble of particles wanders within a site of reconnection by moving along chaotic orbits, the behaviour of these particles as regards the gain or loss of kinetic energy mimics a stochastic process. This seems also to be a natural framework for the discussion of the acceleration process in multiple loop coalescence models for flares (e.g. Tajima et al. 1987; Kliem, Karlicky & Benz 2000), in which the final spectra from test particle distributions (e.g. fig. 15 of Tajima et al. 1987) are qualitatively similar to the spectra shown in Section 4 above.

The particle dynamics in the adiabatic region of X-points (away from the X-lines) has similarities with the RCS case that are worth mentioning. The growth of the velocity component parallel to the magnetic field results in the appearance, in both cases, of phenomena like separatrix jets, small exit pitch angles and, if a longitudinal magnetic field component is present, charge separation (Zhu & Parks 1993; Vekstein & Browning 1997; Browning & Vekstein 2001; Zharkova & Gordovskyy 2004, 2005, and the present study).

The maximum energy gain of the particles in X-points depends on whether the particles enter and for how long in the non-adiabatic region. The energy gain of the particles entering in the region determines the upper cut-off limit of the final energy distribution. Contrary to the RCS case (see Fig. 1 for electrons), this limit is not affected by a non-zero longitudinal magnetic field (Browning & Vekstein 2001; Hannah & Fletcher 2006). The latter can only shift the shape of the particles' kinetic energy distribution towards higher energies (Mori et al. 1998; Browning & Vekstein 2001; Hannah & Fletcher 2006) by influencing the dynamics of the particles not approaching the non-adiabatic region in a way similar to the dynamics of particles within an RCS.

Finally, we stress that, as exemplified in Section 5 above, a detailed comparison of what a model gives with observational data is possible only after the particles' energy distributions are convolved with a kernel incorporating a model of radiation of the energetic particles, such as the thick target model. In our case, this convolution greatly distorts the final spectra. It is reasonable to anticipate that such distortions should be present in almost any model combining the particle acceleration and radiation processes.

ACKNOWLEDGMENTS

This work was supported in part by the Research Committee of the Academy of Athens. We wish to thank Dr N. Vilmer for kindly providing the code of calculation of X-ray spectra in the thick target model and Dr I. Contopoulos for stimulating discussions on the problem of magnetic reconnection.

REFERENCES

Anastasiadis A., Vlahos L., 1991, *A&A*, 245, 271
 Anastasiadis A., Vlahos L., 1994, *ApJ*, 428, 819
 Anastasiadis A., Vlahos L., Georgoulis M. K., 1997, *ApJ*, 489, 367

Anastasiadis A., Gontikakis C., Vlimer N., Vlahos L., 2004, *A&A*, 422, 323
 Arnold V. I., Novikov S. P., 2000, *Dynamical Systems VII. Encyclopaedia of Mathematical Sciences*, Vol. 16. Springer-Verlag, Berlin
 Aschwanden M. J., Montello M., Dennis B. R., Benz A. O., 1995, *ApJ*, 440, 394
 Aschwanden M. J., Tarbell T. D., Nightingale R. W., Schrijver C. J., Title A., Kankelborg C. C., Martens P., Warren H., 2000, *ApJ*, 535, 1047
 Benz A. O., 1985, *Sol. Phys.*, 96, 357
 Benz A. O., Aschwanden M. J., 1992, in Svestka Z., Jackson B. V., Machado M. E., eds, *Lecture Notes in Physics*, Vol. 399. Springer-Verlag, New York, p. 106
 Brown J. C., 1971, *Sol. Phys.*, 18, 489
 Browning P. K., Vekstein G. E., 2001, *J. Geophys. Res.*, 106, 18677
 Bruhwiler D. L., Zweibel E. G., 1992, *J. Geophys. Res.*, 97, 10825
 Büchner J., Zelenyi L. M., 1991, *Adv. Space Res.*, 11, 177
 Bulanov S. V., 1980, *Sov. Astron. Lett.*, 6, 206
 Burkhardt G. R., Drake J. F., Chen J., 1990, *J. Geophys. Res.*, 95, 18833
 Craig I. J. D., Litvinenko Y. E., 2002, *ApJ*, 570, 387
 Crosby N. B., Aschwanden M. J., Dennis R. B., 1993, *Sol. Phys.*, 143, 275
 Crosby N. B., Vilmer N., Lund N., Sunyaev R., 1998, *A&A*, 334, 299
 Dalla S., Browning P. K., 2005, *A&A*, 436, 1103
 Deeg H. J., Borovsky J. E., Duric N., 1991, *Phys. Fluids*, B3, 2660
 Dennis B. R., 1985, *Sol. Phys.*, 100, 465
 Efthymiopoulos C., Gontikakis C., Anastasiadis A., 2005, *A&A*, 443, 663
 Fletcher L., Petkaki P., 1997, *Sol. Phys.*, 172, 267
 Gontikakis C., Efthymiopoulos C., Anastasiadis A., 2006, *MNRAS*, 368, 293
 Hamilton B., McClements K. G., Fletcher L., Thyagaraja A., 2003, *Sol. Phys.*, 214, 339
 Hamilton B., Fletcher L., McClements K. G., Thyagaraja A., 2005, *ApJ*, 625, 496
 Hannah I. G., Fletcher L., 2006, *Sol. Phys.*, 236, 59
 Hannah I. G., Fletcher L., Hendry M. A., 2002, in *ESA SP-506, Solar Variability: From Core to Outer Frontiers*. ESA Publications Division, Noordwijk
 Heerikhuisen J., Litvinenko Y. E., Craig I. J. D., 2002, *ApJ*, 566, 512
 Horiuchi R., Sato T., 1997, *Phys. Plasmas*, 4, 277
 Kliem B., 1994, *ApJS*, 90, 719
 Kliem M., Karlicky M., Benz A. O., 2000, *A&A*, 360, 715
 Krucker S., Benz A. O., 1998, 501, 213
 Litvinenko Y. E., 1996, *ApJ*, 462, 997
 Litvinenko Y. E., Craig I. J. D., 1999, *Sol. Phys.*, 189, 315
 Litvinenko Y. E., Somov B., 1993, *Sol. Phys.*, 146, 127
 Martens P., 1988, *ApJ*, 330, 131
 Martens P., Young A., 1990, *ApJS*, 73, 333
 Mori K. I., Sakai J. I., Zhao J., 1998, *ApJ*, 494, 430
 Moses R. W., Finn J. M., Ling K. M., 1993, *J. Geophys. Res.*, 98, 4013
 Nitta N., Dennis B. R., Kiplinger A. L., 1990, *ApJ*, 353, 313
 Parker E. N., 1988, *ApJ*, 330, 474
 Petkaki P., MacKinnon A. L., 1997, *Sol. Phys.*, 172, 279
 Somov B. V., 1992, *Physical Processes in Solar Flares*. Kluwer, Dordrecht, Holland
 Speiser T. W., 1965, *J. Geophys. Res.*, 70, 4219
 Tajima T., Sakai J., Nakajima H., Kosugi T., Brunel F., Kundu M. R., 1987, *ApJ*, 321, 1031
 Vekstein G. E., Browning P. K., 1997, *Phys. Plasmas*, 4, 2261
 Vilmer N., Trotter G., Kane S. R., 1982, *A&A*, 108, 306
 Vlahos L., Isleri H., Lepreti F., 2004, *ApJ*, 608, 540
 Wood P., Neukirch T., 2005, *Sol. Phys.*, 226, 73
 Zharkova V., Gordovskyy M., 2004, *ApJ*, 604, 884
 Zharkova V., Gordovskyy M., 2005, *MNRAS*, 356, 1107
 Zhu Z., Parks G., 1993, *J. Geophys. Res.*, 98, 7603

This paper has been typeset from a $\text{\TeX}/\text{\LaTeX}$ file prepared by the author.